



## Hydrodeoxygenation of furans over Pd-FeO<sub>x</sub>/SiO<sub>2</sub> catalyst under atmospheric pressure



Jinfan Yang <sup>a,b,1</sup>, Shanshan Li <sup>a,c,1</sup>, Leilei Zhang <sup>a</sup>, Xiaoyan Liu <sup>a,d</sup>, Junhu Wang <sup>a</sup>, Xiaoli Pan <sup>a</sup>, Ning Li <sup>a,d,\*</sup>, Aiqin Wang <sup>a,d</sup>, Yu Cong <sup>a</sup>, Xiaodong Wang <sup>a</sup>, Tao Zhang <sup>a,d,\*</sup>

<sup>a</sup> State Key Laboratory of Catalysis, Dalian Institute of Chemical Physics, Chinese Academy of Sciences, Dalian 116023, China

<sup>b</sup> Shaanxi University of Science & Technology, College of Light Industry & Energy, Xi'an 710021, China

<sup>c</sup> University of Chinese Academy of Sciences, Beijing, 100049, China

<sup>d</sup> iChEM (Collaborative Innovation Center of Chemistry for Energy Materials), Dalian Institute of Chemical Physics, Chinese Academy of Sciences, Dalian 116023, China

### ARTICLE INFO

#### Article history:

Received 10 June 2016

Received in revised form 31 July 2016

Accepted 19 August 2016

Available online 20 August 2016

#### Keywords:

Diesel and jet fuel

Solvent-free

Hydrodeoxygenation

Furans

Pd-FeO<sub>x</sub>/SiO<sub>2</sub>

### ABSTRACT

For the first time, the Pd/SiO<sub>2</sub> which was modified by FeO<sub>x</sub> species (Pd-FeO<sub>x</sub>/SiO<sub>2</sub>) was reported as an active catalyst for the solvent-free hydrodeoxygenation (HDO) of the aldol condensation product of furfural and methyl-isobutylketone (MIBK). The presence of iron species not only restrains the C–C cleavage (decarbonylation and retro-aldol condensation) over the Pd/SiO<sub>2</sub> catalyst but also decreases the hydrogen pressure which is needed for the total HDO of aldol condensation product over the Pd/SiO<sub>2</sub> catalyst. Compared with the Pd/SiO<sub>2</sub> catalyst, the Pd-FeO<sub>x</sub>/SiO<sub>2</sub> catalyst also exhibited higher activity for the HDO of other furan compounds under atmospheric pressure. Over the 5%Pd-2.5%FeO<sub>x</sub>/SiO<sub>2</sub> catalyst, complete conversion of feedstocks and high carbon yields of jet fuel range alkanes (87–94%) can be achieved by the atmospheric HDO of a series of furan compounds at 623 K or 573 K. From the results of XRD, STEM, CO chemisorption, FT-IR, EXAFS, H<sub>2</sub>-TPR, *in-situ* XPS and *quasi-in-situ* Mössbauer spectra, it was noticed that the modification of iron species decreases the coordination number of Pd–Pd on the Pd/SiO<sub>2</sub> catalyst, which may restrain the decarbonylation during the HDO process. The presence of Pd promotes the reduction of iron species and the generation of Pd–Fe alloy. Both effects may be the reasons why the Pd-FeO<sub>x</sub>/SiO<sub>2</sub> catalyst is more active than Pd/SiO<sub>2</sub> in the solvent-free HDO of furan compounds under atmospheric pressure.

© 2016 Elsevier B.V. All rights reserved.

### 1. Introduction

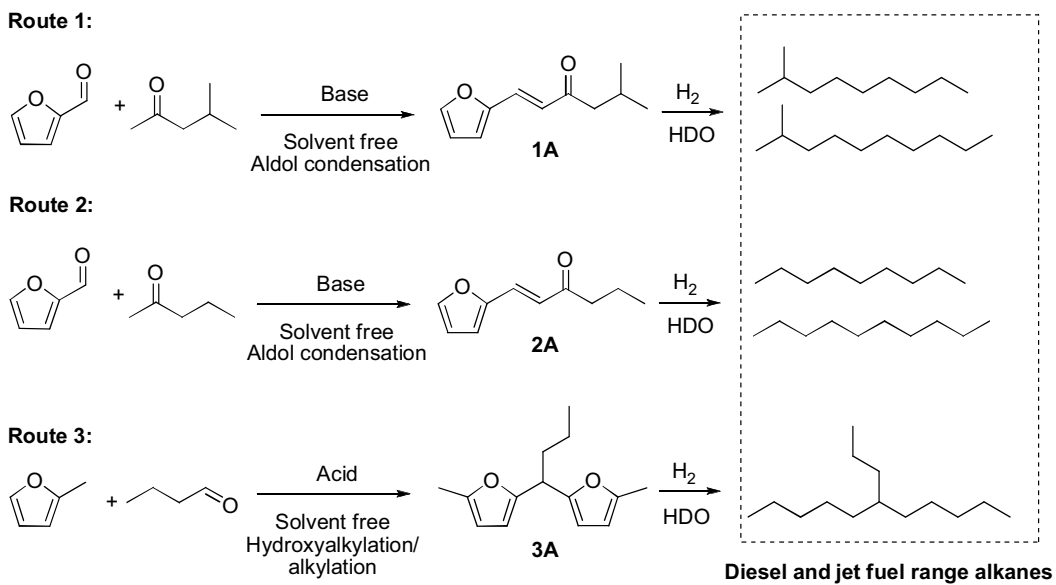
With the increase of social concern about the energy and environmental problems we are facing today, the catalytic conversion of renewable biomass to fuels [1–5] and chemicals [6–10] has attracted tremendous attention. Lignocellulose is the main component of the agricultural wastes and forestry residues. Diesel and jet fuel are two kinds of often used liquid fuels. In recent years, there were a lot of reports about the synthesis of diesel and jet fuel range hydrocarbons using the platform compounds which can be obtained from lignocellulose by chemical or biological methods [11–16].

Furan compounds (such as furan, furfural, 2-methylfuran, 5-hydroxymethylfurfural, 5-methylfurfural etc.) are a family of celullosic or hemicelullosic platform compounds which were often used in the synthesis of renewable diesel and jet fuel. In the previous work of Dumesic [12,17–19], Huber [20–22], Corma [23–26] and other groups [27–35], several routes to diesel and jet fuel range alkanes have been developed by the C–C coupling reactions (e.g. aldol condensation, hydroxyalkylation/alkylation, alkylation, benzoic condensation) of furan compounds followed by hydrodeoxygenation (HDO). In the previous reports on the hydrodeoxygenation (HDO) of furan-based diesel and jet fuel precursors from the C–C coupling reactions (see Table S1 in supporting information for a summary of recent literature), the reactions were conducted at high temperature (433–643 K) and high hydrogen pressure (2–6 MPa), which will lead to high facility cost and energy consumption in real application. To decrease the energy consumption and the cost of facility, it is imperative to explore new method [36–38] or effective catalyst [31,39]

\* Corresponding authors at: State Key Laboratory of Catalysis, Dalian Institute of Chemical Physics, Chinese Academy of Sciences, Dalian 116023, China

E-mail addresses: [lining@dicp.ac.cn](mailto:lining@dicp.ac.cn) (N. Li), [taozhang@dicp.ac.cn](mailto:taozhang@dicp.ac.cn) (T. Zhang).

<sup>1</sup> These authors contributed equally.



**Scheme 1.** Strategies for the synthesis of diesel and jet fuel range branched alkanes.

which can be operated under mild conditions. Moreover, HDO is a very important reaction in biomass conversion, the exploration new strategy [40–44] or cost effective catalyst [45–47] for the HDO process also has great significance. So far, most of the reported work is concentrated on decreasing the HDO temperature of furan compounds. To the best of our knowledge, there is no report about the synthesis of diesel and jet fuel range alkanes by the HDO of furan compounds under atmospheric hydrogen pressure.

In this work, the Pd/SiO<sub>2</sub> catalyst which was modified by FeO<sub>x</sub> species (Pd-FeO<sub>x</sub>/SiO<sub>2</sub>) was first reported to be an effective catalyst for the solvent-free HDO of several lignocellulose derived furan compounds under atmospheric pressure. To figure out the reasons for the excellent performance of the Pd-FeO<sub>x</sub>/SiO<sub>2</sub>, the catalysts were characterized by a series of technologies.

## 2. Experimental

### 2.1. Preparation of catalysts

The Pd/SiO<sub>2</sub> and Pd/C catalysts used in this work were prepared by the incipient wetness impregnation of SiO<sub>2</sub> (Qingdao Ocean Chemical Ltd., BET surface area 509 m<sup>2</sup> g<sup>-1</sup>) and the HNO<sub>3</sub> treated active carbon (supplied by the NORIT Company. Specific BET surface area: 762 m<sup>2</sup> g<sup>-1</sup>) with the aqueous solution of PdCl<sub>2</sub>, respectively. The Pd-FeO<sub>x</sub>/SiO<sub>2</sub> catalysts were prepared by the incipient wetness co-impregnation of SiO<sub>2</sub> with the aqueous solution of PdCl<sub>2</sub> and Fe(NO<sub>3</sub>)<sub>3</sub>•9H<sub>2</sub>O. The theoretical weight percentages of Pd and Fe in the catalysts were indicated in the names of these catalysts. For example, the 5%Pd-2.5%FeO<sub>x</sub>/SiO<sub>2</sub> denotes the catalyst which contains 5% weight percentage of Pd and 2.5% weight percentage of Fe. To facilitate comparison, we also prepared the FeO<sub>x</sub>/SiO<sub>2</sub> catalyst by the incipient wetness impregnation of SiO<sub>2</sub> with the aqueous solution of Fe(NO<sub>3</sub>)<sub>3</sub>•9H<sub>2</sub>O. The theoretical weight percentage of Fe in the catalyst is 10% (denoted as 10% FeO<sub>x</sub>/SiO<sub>2</sub>). The products were dried at 393 K for 12 h, reduced by hydrogen flow at 623 K (the same temperature as that used in most of the HDO tests) for 2 h to reach a steady state, cooled down to room temperature in hydrogen flow, and passivated with 1 vol.% O<sub>2</sub> in N<sub>2</sub>.

## 2.2. Characterization

### 2.2.1. X-ray diffraction (XRD)

XRD patterns of the Pd/SiO<sub>2</sub>, Pd-FeO<sub>x</sub>/SiO<sub>2</sub> and FeO<sub>x</sub>/SiO<sub>2</sub> catalysts were recorded by PANalytical X'Pert-Pro powder X-ray diffractometer using Cu K $\alpha$  radiation ( $\lambda = 0.1541$  nm), operating at 40 kV and 40 mA (intended wavelength type, K $\alpha$ 1; K $\alpha$ 2/K $\alpha$ 1 intensity ratio, 0.50) in the angle interval 5–80° (2 $\theta$ ), with a step size of 0.0334° (2 $\theta$ ) and a counting time of 20.32 s per step. The scanning speed was chosen as 0.2° min<sup>-1</sup>. The incident beam passed through a 0.04 rad Soller slit, a 10 mm fixed mask, a 1° antiscatter slit, and a 1/2° divergence slit. Before the tests, the catalysts were reduced by H<sub>2</sub> flow at 623 K for 2 h.

### 2.2.2. Scanning transmission electron microscope (STEM)

The scanning transmission electron microscopy images with the energy dispersive X-ray (STEM-EDX) spectra for elemental analysis in point, line or area scan modes were conducted with an energy dispersive spectroscopy analyzer which was attached to a JEM-2100F equipped with a STEM dark-field detector under the accelerating voltage of 200 kV. The high-resolution TEM (HRTEM) images of the catalysts were obtained from a JEM-2100F field emission electronic microscope operated at 200 kV. Before the test, the catalysts were reduced by H<sub>2</sub> at 623 K for 2 h. The reduced catalysts were ultrasonically dispersed in ethanol, put dropwise onto the microgrid carbon polymer supported on copper grid and thoroughly dried for characterization.

### 2.2.3. CO chemisorption

The CO chemisorption of the Pd/SiO<sub>2</sub> and Pd-FeO<sub>x</sub>/SiO<sub>2</sub> catalysts was carried out with a Micromeritics AutoChem II 2920 Automated Catalyst Characterization System. The Pd dispersions on the catalysts were calculated according to the molar ratios of the chemically adsorbed CO on the catalysts and the Pd in the catalysts (assuming that the stoichiometry of chemically adsorbed CO to surface Pd atom is one). These values correspond to the ratio of surface Pd atoms to total Pd atoms. Before each test, the sample was heated in He flow at 423 K for 1 h to remove the physically adsorbed water. After this pretreatment, the sample was reduced in H<sub>2</sub> flow at 623 K for 2 h, purged in He flow at 633 K for 1 h and cooled down in He

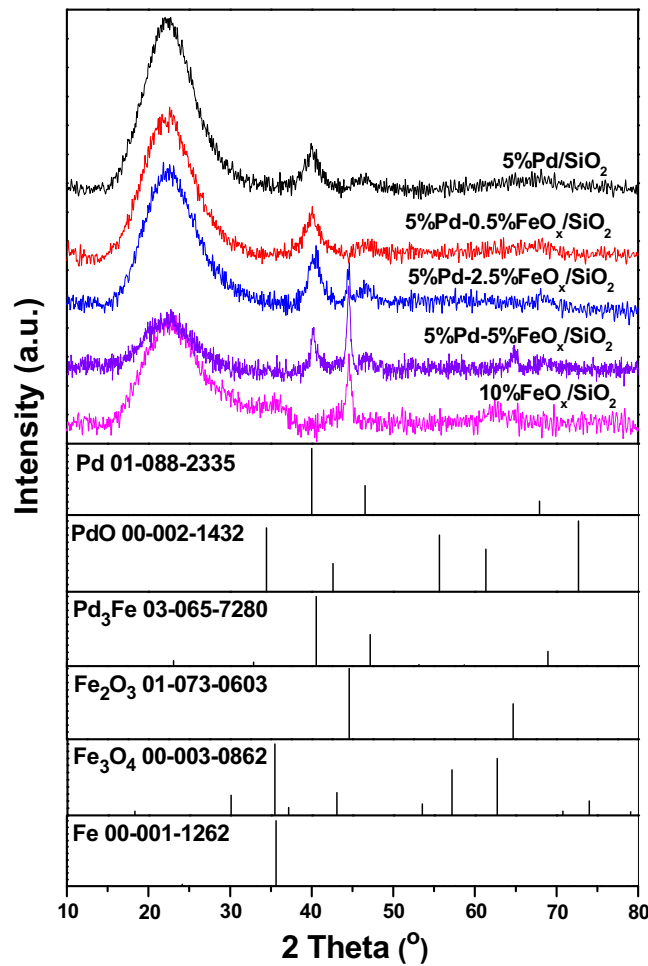


Fig. 1. XRD patterns of the Pd/SiO<sub>2</sub> and Pd-FeO<sub>x</sub>/SiO<sub>2</sub> catalysts.

flow to 313 K. After the stabilization of baseline, the CO adsorption was carried out by the pulse adsorption of 5% CO in He.

#### 2.2.4. Fourier transform-infrared (FT-IR) spectrum for CO adsorption

The FT-IR spectra with CO as the probe molecule were recorded on a Bruker spectrometer (EQUINOX55) equipped with a MCT detector at a spectral resolution of 4 cm<sup>-1</sup> and an accumulation of 120 scans. Before the experiment, the samples were pre-reduced by hydrogen flow at 623 K for 2 h, evacuated at the same temperature for 1 h and cooled to room temperature. At this stage, the spectrum was recorded as the background reference. Subsequently, CO was introduced ( $2 \times 10^3$  Pa) at room temperature for 5 min, followed by evacuation for 30 min at the same temperature. The spectra were collected and subtracted with the background References

#### 2.2.5. Extended X-ray absorption fine structure spectrum (EXAFS)

The X-ray absorption spectra (XAS) including X-ray absorption near-edge structure (XANES) and extended X-ray absorption fine structure (EXAFS) spectra at the K-edge of Fe were recorded at the BL14W1 at Shanghai Synchrotron Radiation Facility (SSRF), Shanghai Institute of Applied Physics (SINAP), China. A double Si (111)-crystal monochromator was used for energy selection. The energy was calibrated by Fe foil. Before the experiment, the sample was reduced at 623 K for 2 h and sealed into Kapton film in the glove box without exposure to the air. The spectra were collected at room temperature under the transmission mode with the

solid state detector. The data were analyzed by the Athena software packages [48].

#### 2.2.6. H<sub>2</sub>-temperature programmed reduction (H<sub>2</sub>-TPR)

H<sub>2</sub>-TPR tests of the Pd/SiO<sub>2</sub>, Pd-FeO<sub>x</sub>/SiO<sub>2</sub> and FeO<sub>x</sub>/SiO<sub>2</sub> catalysts were carried out by the Micromeritics AutoChem II 2920 Automated Catalyst Characterization System. Before the reduction, the samples were heated in Ar flow at 473 K for 1 h to remove physically adsorbed water. Subsequently, the carrier gas was switched from pure Ar to 10% H<sub>2</sub> in Ar. After the stabilization of base line, the samples were heated from 223 K to 1073 K at the heating rate of 10 K min<sup>-1</sup>.

#### 2.2.7. In-situ X-ray photoelectron spectroscopy (XPS)

In-situ XPS analysis was conducted with an ESCALAB 250Xi spectrometer using Al K $\alpha$  X-ray source with pass energy of 20 eV and base pressure of analysis chamber greater than  $1 \times 10^{-8}$  Pa. Before the analysis, the samples were pre-reduced by hydrogen at 623 K for 2 h.

#### 2.2.8. Quasi-in-situ Mössbauer spectra

Quasi-in-situ <sup>57</sup>Fe Mössbauer spectra of the 10%FeO<sub>x</sub>/SiO<sub>2</sub> and 5%Pd-2.5%FeO<sub>x</sub>/SiO<sub>2</sub> catalysts were recorded at room temperature by a Topologic 500A spectrometer and a proportional counter. <sup>57</sup>Co(Rh) moving with a constant acceleration mode was used as the  $\gamma$ -ray radioactive source. In a typical test, the catalyst was loaded into a U-shaped quartz reactor, reduced in H<sub>2</sub> flow at 623 K for 2 h and then cooled down to 293 K in He flow. Subsequently, the quartz

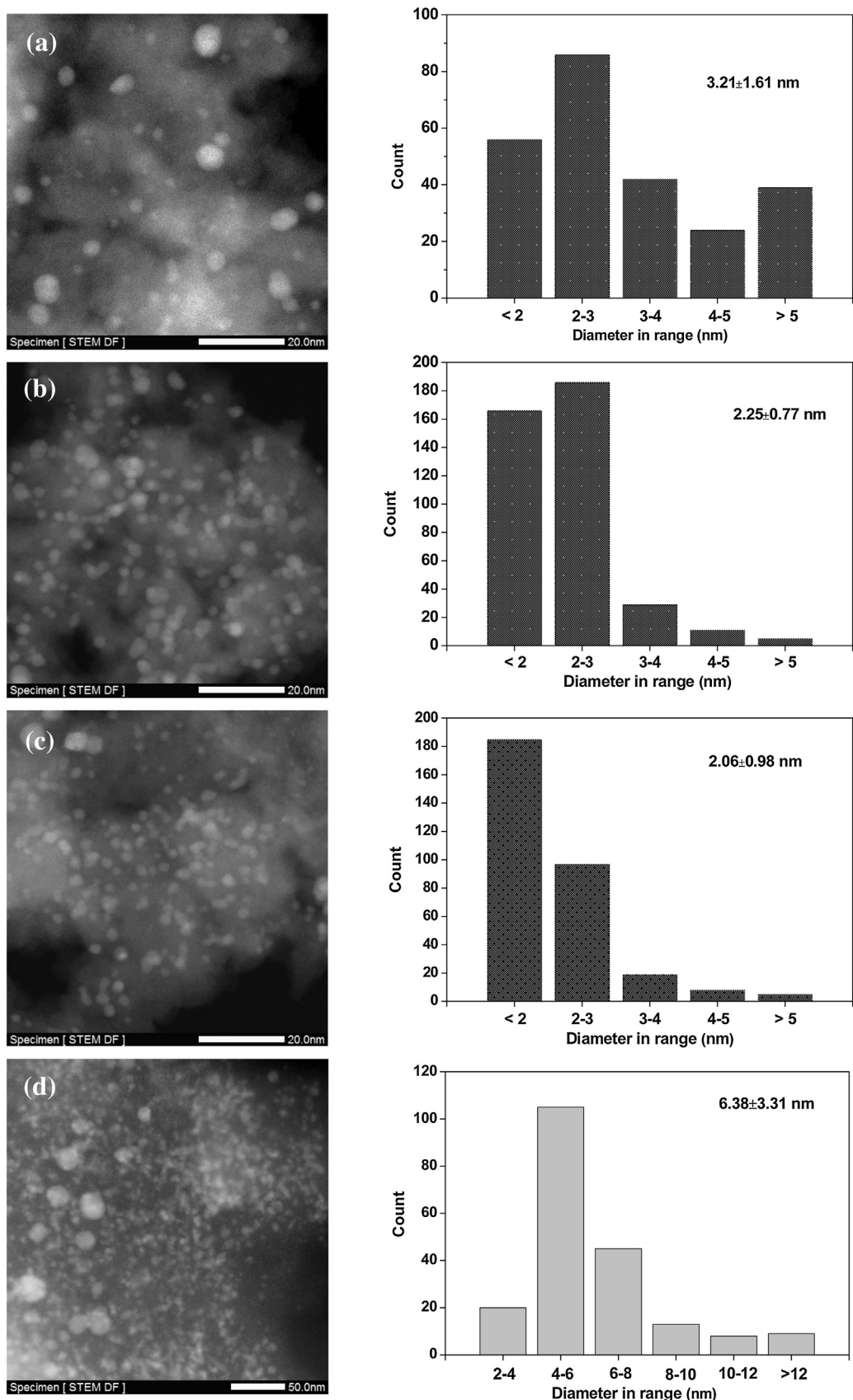


**Fig. 2.** STEM images of (a) 5%Pd/SiO<sub>2</sub>, (b) 5%Pd-0.5%FeO<sub>x</sub>/SiO<sub>2</sub>, (c) 5%Pd-2.5%FeO<sub>x</sub>/SiO<sub>2</sub> and (d) 5%Pd-5%FeO<sub>x</sub>/SiO<sub>2</sub> catalysts.

reactor was sealed (to ensure the sample isolated from atmospheric air) and transferred into a glove box under argon atmosphere. In the glove box, the catalyst was put into the sample cell, taped and then taken out for the measurement. The velocity was calibrated by a standard  $\alpha$ -iron foil. The spectra were fitted with the appropriate superpositions of Lorentzian lines using the Mössbauer 4.0pre program. In this way, the  $^{57}\text{Fe}$  Mössbauer spectral parameters could be determined, including the isomer shift (IS), the electric quadrupole splitting (QS) and the relative abundance of different components.

### 2.3. Activity tests

The solvent-free HDO of the furan compounds was carried out in a stainless steel tubular flow reactor described in our previous work [49–51]. In real application, the solvent-free HDO process is advantageous because it can decrease the energy consumption while heating feedstock to reaction temperature and increase facility efficiency. For each test, 1.8 g catalyst was used. Before the test, the catalyst was heated to 623 K in hydrogen flow and stabilized at this temperature for 0.5 h. The 1-(furan-2-yl)-5-methylhex-1-en-3-one, 1-(furan-2-yl)hex-1-en-3-one and the 5,5'-(butane-1,1-diyl)bis(2-methylfuran) (i.e. **1A**, **2A** and **3A** in Scheme 1) were fed into the reactor from the bottom of the reactor by a HPLC pump (at a rate of 0.04 mL min<sup>−1</sup>) along with hydrogen (at a flow rate of 110 mL min<sup>−1</sup> at STP). The preparation methods of **1A**, **2A** and **3A** were described in supporting information. For **1A** and **2A**, the HDO experiments were conducted at 623 K under a hydrogen pressure of 6 MPa (or 0.1 MPa). Compared with **1A** or **2A**, the HDO of **3A** is relatively easier. This is because the furan ring opening reaction/hydrogenation of **1A** or **2A** may lead to the generation of primary alcohol, while the furan ring opening reaction/hydrogenation of **3A** only produces secondary alcohol. According to literature [52], the HDO of primary alcohols is more difficult than secondary alcohols. Therefore, the HDO of **3A** were conducted at 573 K under a hydrogen pressure of 0.1 MPa. The products from the outlet of tubular reactor passed through a gas-liquid separator and became two phases. The gaseous products flowed through a back pressure regulator (which was used to maintain the pressure of reaction system) and were analyzed on-line by an Agilent 6890N GC equipped with a TCD detector and a FID detector. Liquid products were drained from the gas-liquid separator after the reaction was carried out for 5 h and analyzed by another Agilent 7890A GC equipped with a FID detector.

## 3. Results

### 3.1. Characterization

From the XRD patterns of the Pd/SiO<sub>2</sub> and Pd-FeO<sub>x</sub>/SiO<sub>2</sub> catalysts shown in Fig. 1, only the peaks of SiO<sub>2</sub> support and metallic Pd (JCPDS 00-001-1262) or Pd<sub>3</sub>Fe (JCPDS 00-001-1262) phases were observed. No peak of Pd (or Fe) oxide phase was noticed. In the XRD patterns of the 5%Pd-2.5%FeO<sub>x</sub>/SiO<sub>2</sub> and 5%Pd-5%FeO<sub>x</sub>/SiO<sub>2</sub> catalysts, small peaks at 44.5° can also be observed. According to the result of *quasi-in-situ* Mössbauer spectra (which will be described later), these peaks can be attributed to iron-rich Pd-Fe alloy (JCPDS 03-065-6583). In the XRD pattern of the 10%FeO<sub>x</sub>/SiO<sub>2</sub> catalyst, a peak at 44.6° can be observed. This peak can be assigned to metallic Fe phase (JCPDS 00-001-1262).

Fig. 2 shows the STEM images of the Pd/SiO<sub>2</sub> and Pd-FeO<sub>x</sub>/SiO<sub>2</sub> catalysts. From it, we can see that the modification of the Pd/SiO<sub>2</sub> with small amount of iron species (iron content less than 2.5 wt.%) will lead to the generation of Pd-Fe alloy with lower average particle sizes (see Table 1). When the iron content of the Pd-FeO<sub>x</sub>/SiO<sub>2</sub> catalyst is higher than 2.5 wt.%, further increase of iron content

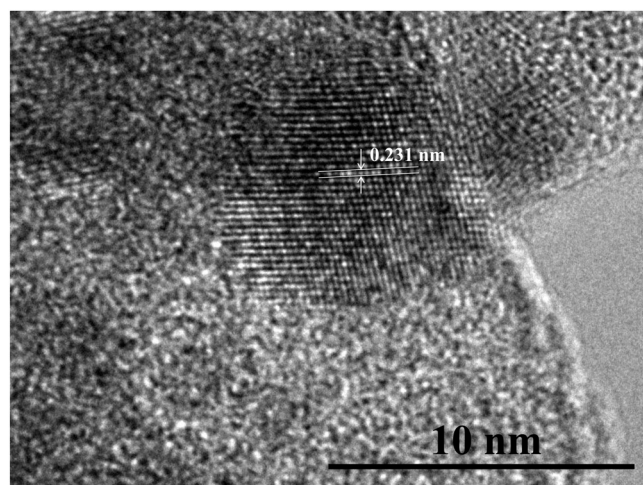


Fig. 3. HRTEM image of the 5%Pd-2.5%FeO<sub>x</sub>/SiO<sub>2</sub> catalyst.

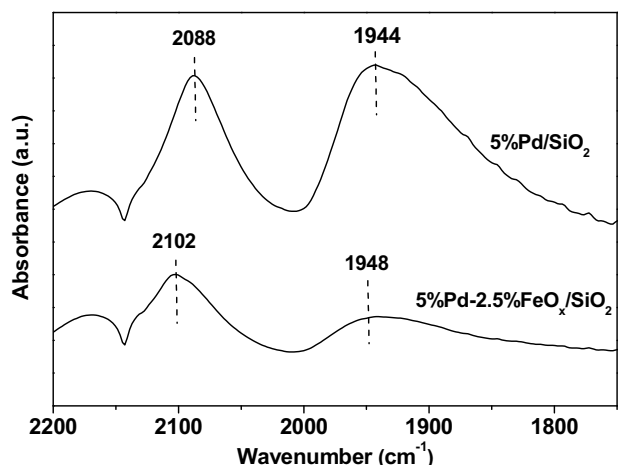


Fig. 4. FT-IR spectra of the 5%Pd/SiO<sub>2</sub> and 5%Pd-2.5%FeO<sub>x</sub>/SiO<sub>2</sub> catalysts after CO adsorption and evacuation at room temperature.

to 5 wt.% will lead to the aggregation of Pd-Fe alloy particles. The STEM-EDX spectra of the Pd-FeO<sub>x</sub>/SiO<sub>2</sub> catalysts were shown in Fig. S1–S5. Although the atomic ratio of Fe to Pd varies from one particle to another one, there is always iron and palladium species on the particles which were randomly chosen on the surfaces of the 5%Pd-0.5%FeO<sub>x</sub>/SiO<sub>2</sub> and 5%Pd-2.5%FeO<sub>x</sub>/SiO<sub>2</sub> catalysts. From this result, we can see that the iron and palladium species on the Pd-FeO<sub>x</sub>/SiO<sub>2</sub> catalysts are closely contacted.

According to Fig. 3, the lattice spacing of the metallic particles on the 5%Pd-2.5%FeO<sub>x</sub>/SiO<sub>2</sub> catalyst was estimated as 2.31 Å which is bigger than the lattice spacing of the Pd (111) plane (2.24 Å) but smaller than that of Fe (111) plane (2.89 Å). This may be considered as another proof for the generation of Pd-Fe alloy with the lattice spacing between Pd and Fe.

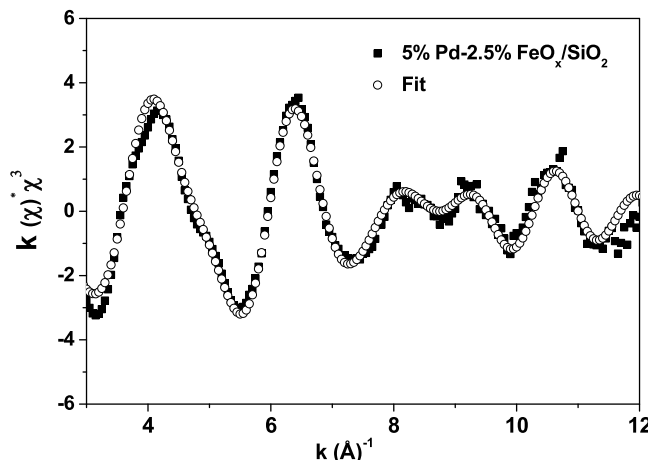
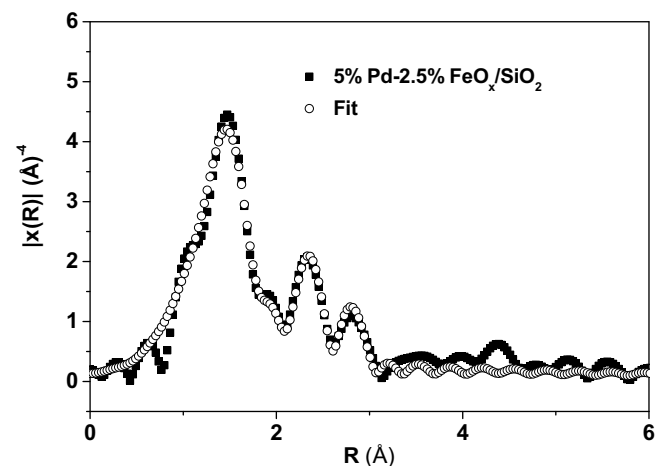
From the CO chemisorption results listed in Table 1, the Pd dispersion on the 5%Pd/SiO<sub>2</sub> catalyst decreases after the modification of iron species. This phenomenon becomes more evident with the increasing of iron content. According to the results of STEM, the average metal particle size decreases after the modification of the Pd/SiO<sub>2</sub> catalyst with iron species. Therefore, such a decrease of CO adsorption can be rationalized either by the dilution effect caused by the formation of Pd-Fe alloy [54] or by the coverage of Pd (or Pd-Fe alloy) particles with FeO<sub>x</sub> clusters [55,56].

Fig. 4 shows the FT-IR spectra of the 5%Pd/SiO<sub>2</sub> and 5%Pd-2.5%FeO<sub>x</sub>/SiO<sub>2</sub> catalysts after CO adsorption and evacuation at

**Table 1**

The actual metal contents, average metal particle sizes and metal dispersions on different catalysts.

Catalyst	Actual metal content (wt.%) <sup>a</sup>		Average metal particle size (nm) <sup>b</sup>	CO chemisorption ( $\mu\text{mol g}^{-1}$ )	Metal dispersion (%) <sup>c</sup>
	Pd	Fe			
5%Pd/SiO <sub>2</sub>	5.1	–	3.21 ± 1.61	136.0	28.0
5%Pd-0.5%FeO <sub>x</sub> /SiO <sub>2</sub>	4.8	0.4	2.25 ± 0.77	73.8	15.0
5%Pd-2.5%FeO <sub>x</sub> /SiO <sub>2</sub>	4.9	2.3	2.06 ± 0.98	55.0	11.7
5%Pd-5%FeO <sub>x</sub> /SiO <sub>2</sub>	5.3	5.6	6.38 ± 3.31	12.8	2.7

<sup>a</sup> The actual metal contents in the catalysts were measured by ICP analysis.<sup>b</sup> The average metal particle sizes were estimated according to the STEM results.<sup>c</sup> The metal dispersions were calculated according to the CO chemisorption results.**Fig. 5.** Experimental and theoretical oscillations in  $k$ -space of the 5%Pd-2.5%FeO<sub>x</sub>/SiO<sub>2</sub> catalyst.**Fig. 6.** Fourier transform of  $k^3$ -weighted EXAFS spectra of the 5%Pd-2.5%FeO<sub>x</sub>/SiO<sub>2</sub> catalyst: experimental vs. data fitting results.

room temperature. From them, two bands at the wavenumbers around 2100  $\text{cm}^{-1}$  and 1950  $\text{cm}^{-1}$  can be observed. According to literature [54,57], the band around 2100  $\text{cm}^{-1}$  can be assigned to the CO which is linearly adsorbed on Pd sites, while the band around 1950  $\text{cm}^{-1}$  can be attributed to the bridge bonded CO which is adsorbed on the Pd sites. After the modification of the Pd/SiO<sub>2</sub> catalyst with iron species, three changes were observed. 1) Decrease of the intensities of two bands from the linear and bridge bonded CO on Pd sites. This result further confirms that the modification of FeO<sub>x</sub> species decreases the CO chemisorption on the surface of the Pd/SiO<sub>2</sub> catalyst. 2) Red shifts of the CO adsorption bands to higher wavenumbers. This phenomenon can be explained by the strong interaction between the palladium and iron species [53,58]. 3) Decrease of the ratio between the bridge and linearly bonded CO which is indicated by the area ratio of the bands at 2100  $\text{cm}^{-1}$  and 1950  $\text{cm}^{-1}$ . According to literature [54], the CO is mainly adsorbed on pure Pd monocrystalline surface in bridged form. In contrast, linearly adsorbed CO can be observed on small Pd particles due to the higher fraction of low-coordinated surface Pd atoms. Based on the FT-IR result obtained in this work, we think that the modification of FeO<sub>x</sub> species decreases the interactions between the surface Pd atoms and makes them more isolated. As a result, the linearly bonded CO is predominant over the bridge bonded CO on the surface of the Pd-FeO<sub>x</sub>/SiO<sub>2</sub> catalyst.

The Fe K-edge EXAFS results of the 5%Pd-2.5%FeO<sub>x</sub>/SiO<sub>2</sub> catalyst are illustrated in Fig. 5, Fig. 6 and Table 2. The curve fitting analysis indicates the presence of Fe-O, Fe-Fe, Fe-Pd and Fe-O-Fe (denoted as Fe-Fe<sub>long</sub> in Table 2) bonds with the bond distances of 1.92  $\text{\AA}$ , 2.43  $\text{\AA}$ , 2.65  $\text{\AA}$  and 3.04  $\text{\AA}$ , respectively. The presence of Fe-O and Fe-O-Fe bonds indicates that Fe species in the 5%Pd-2.5%FeO<sub>x</sub>/SiO<sub>2</sub> catalyst is not fully reduced to metallic state. The absence of iron oxide peak in XRD pattern of the 5%Pd-2.5%FeO<sub>x</sub>/SiO<sub>2</sub> catalyst can

**Table 2**  
EXAFS data fitting results of the 5%Pd-2.5%FeO<sub>x</sub>/SiO<sub>2</sub> catalyst.

Shell	N	R ( $\text{\AA}$ )	$\sigma^2 \times 10^2$ ( $\text{\AA}^2$ )	$\Delta E_0$ (eV)	r-factor (%)
Fe-O	4.3	1.92	1.19	-11.8	0.27
Fe-Fe	0.3	2.43	1.20	-11.8	
Fe-Pd	2.3	2.65	1.20	-11.8	
Fe-Fe <sub>long</sub>	1.7	3.04	1.20	-11.8	

N, the coordination number for the absorber-backscatterer pair. R, the average absorber–backscatterer distance.  $\sigma^2$ , the Debye–Waller factor.  $\Delta E_0$ , the inner potential correction. The accuracies of the above parameters were estimated as N, ±20%; R, ±1%;  $\sigma^2$ , ±20%;  $\Delta E_0$ , ±20%. The  $\Delta k$  (3.0–12.0  $\text{\AA}^{-1}$ ) and  $\Delta R$  (1.2–3.1  $\text{\AA}$ ) are the data ranges used for data fitting in k-space and R-space, respectively.

be rationalized because iron oxide is highly dispersed on the catalyst. The presence of Fe-Pd bonds means the formation of Pd-Fe alloy in the 5%Pd-2.5%FeO<sub>x</sub>/SiO<sub>2</sub> catalyst. Meanwhile, the presence of Fe-Fe bonds indicates the formation of metallic Fe or iron-rich Pd-Fe alloy on the 5%Pd-2.5%FeO<sub>x</sub>/SiO<sub>2</sub> catalyst, which is consistent with the XRD results.

The H<sub>2</sub>-TPR profiles of the Pd/SiO<sub>2</sub>, Pd-FeO<sub>x</sub>/SiO<sub>2</sub> and FeO<sub>x</sub>/SiO<sub>2</sub> catalysts are shown in Fig. 7. A negative peak centered at 338 K was observed in the H<sub>2</sub>-TPR profile of the 5%Pd/SiO<sub>2</sub> catalyst. According to literature [59], this peak can be attributed to the decomposition of Pd  $\beta$ -hydride. The H<sub>2</sub>-TPR profile of the 10%FeO<sub>x</sub>/SiO<sub>2</sub> catalyst shows an unresolved peak. According to literature [54,60], the H<sub>2</sub> consumption centered at 623 K can be assigned as the reduction of Fe<sub>2</sub>O<sub>3</sub> to Fe<sub>3</sub>O<sub>4</sub>, while the H<sub>2</sub> consumption centered at 873 K can be attributed to the reduction of Fe<sub>3</sub>O<sub>4</sub> to metallic Fe. In the H<sub>2</sub>-TPR profiles of the 5%Pd-0.5%FeO<sub>x</sub>/SiO<sub>2</sub> and 5%Pd-2.5%FeO<sub>x</sub>/SiO<sub>2</sub> catalysts, the negative peak at 623 K still exists, but its intensity decreases with the increment of Fe content in the catalyst. Furthermore, a new peak at 363 K is observed. According to literature [59],

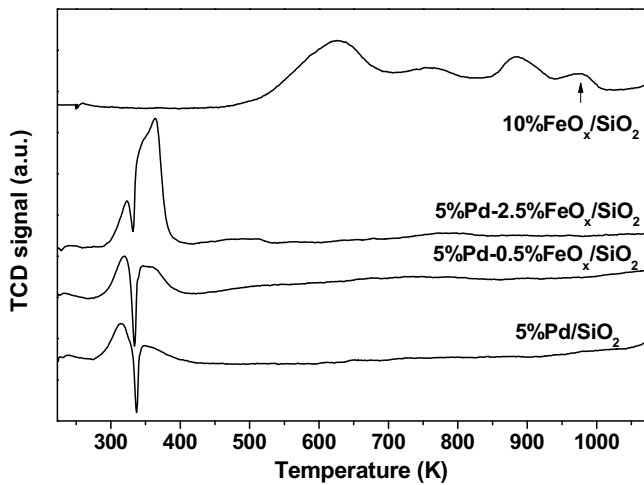


Fig. 7.  $\text{H}_2$ -TPR profiles of the  $\text{Pd}/\text{SiO}_2$ ,  $\text{Pd}-\text{FeO}_x/\text{SiO}_2$  and  $\text{FeO}_x/\text{SiO}_2$  catalysts.

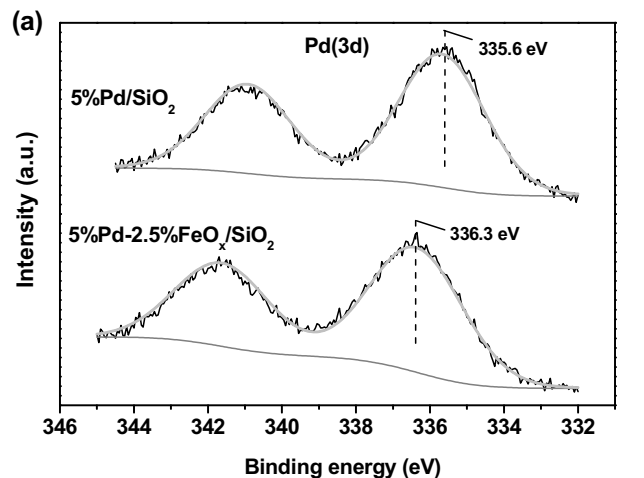


Fig. 8. In-situ XPS spectra of the  $5\% \text{Pd}/\text{SiO}_2$ ,  $5\% \text{Pd}-2.5\% \text{FeO}_x/\text{SiO}_2$  and  $10\% \text{FeO}_x/\text{SiO}_2$  catalysts.

this new peak can be attributed to the formation of Pd-Fe alloy by the hydrogen spillover from Pd particles to the  $\text{FeO}_x$  species attached on them.

According to the binding energies of Pd  $3\text{d}_{5/2}$  (see Fig. 8a), the Pd species in  $5\% \text{Pd}/\text{SiO}_2$  and  $5\% \text{Pd}-2.5\% \text{FeO}_x/\text{SiO}_2$  catalysts mainly exist as metallic state after pretreatment with hydrogen at 623 K.

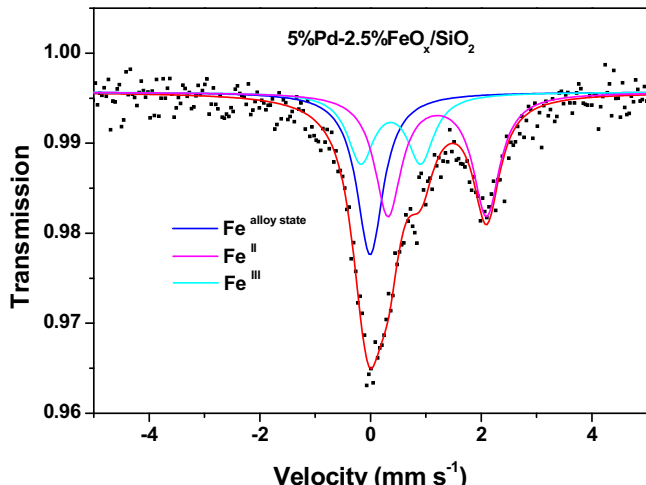


Fig. 9. Room temperature quasi-in-situ  $^{57}\text{Fe}$  Mössbauer spectra of the  $5\% \text{Pd}-2.5\% \text{FeO}_x/\text{SiO}_2$  and  $10\% \text{FeO}_x/\text{SiO}_2$  catalysts.

Compared with the  $5\% \text{Pd}/\text{SiO}_2$  catalyst, the binding energy of Pd  $3\text{d}_{5/2}$  for the  $5\% \text{Pd}-2.5\% \text{FeO}_x/\text{SiO}_2$  catalyst slightly shifts to higher value (from 335.6 eV to 336.3 eV), indicating that there is a strong interaction between the palladium and iron species on the  $5\% \text{Pd}-2.5\% \text{FeO}_x/\text{SiO}_2$  catalyst [61,62]. The binding energies of Fe  $2\text{p}_{3/2}$  for the  $10\% \text{FeO}_x/\text{SiO}_2$  and  $5\% \text{Pd}-2.5\% \text{FeO}_x/\text{SiO}_2$  catalysts are measured as 710.6 eV (see Fig. 8b). This value is between the Fe  $2\text{p}_{3/2}$  binding energies for  $\text{Fe}^{\text{II}}$  (709 eV) and  $\text{Fe}^{\text{III}}$  (711 eV), indicating the surface iron species on the  $10\% \text{FeO}_x/\text{SiO}_2$  and  $5\% \text{Pd}-2.5\% \text{FeO}_x/\text{SiO}_2$  catalysts were partially reduced after pretreatment with hydrogen at 623 K.

Fig. 9 illustrates the quasi-in-situ Mössbauer spectra of the  $5\% \text{Pd}-2.5\% \text{FeO}_x/\text{SiO}_2$  and  $10\% \text{FeO}_x/\text{SiO}_2$  catalysts. According to the literature [54,63] and the fitting results shown in Table 3, Pd-Fe alloy,  $\text{Fe}^{\text{II}}$ , and  $\text{Fe}^{\text{III}}$  species were identified in the spectrum of the  $5\% \text{Pd}-2.5\% \text{FeO}_x/\text{SiO}_2$  catalyst. In contrast,  $\alpha\text{-Fe}$ ,  $\text{Fe}^{\text{II}}$ , and  $\text{Fe}^{\text{III}}$  species were identified in the spectrum of the  $10\% \text{FeO}_x/\text{SiO}_2$  catalyst. These results are consistent with what we observed by XRD, EXAFS,  $\text{H}_2$ -TPR and in-situ XPS tests.

### 3.2. Activity tests

1-(Furan-2-yl)-5-methylhex-1-en-3-one (i.e. **1A** in Scheme 1) is the aldol condensation product of furfural [64] and methyl isobutyl

**Table 3**<sup>57</sup>Fe Mössbauer parameters for the 5%Pd-2.5%Fe/SiO<sub>2</sub> and 10%FeO<sub>x</sub>/SiO<sub>2</sub> catalysts at room temperature.

Sample	Component	IS (mm s <sup>-1</sup> ) <sup>a</sup>	QS (mm s <sup>-1</sup> ) <sup>b</sup>	Line Width (mm s <sup>-1</sup> )	Relative abundance (%)
5%Pd-2.5%FeO <sub>x</sub> /SiO <sub>2</sub>	Fealloystate	-0.01	-	0.58	30.1
	Fe <sup>II</sup>	1.21	1.78	0.58	44.9
	Fe <sup>III</sup>	0.37	1.08	0.58	25
10%FeO <sub>x</sub> /SiO <sub>2</sub>	$\alpha$ -Fe	-0.02	-	0.35	26.7
	Fe <sup>II</sup>	1.01	1.60	0.58	21.4
	Fe <sup>III</sup>	0.34	0.96	0.58	51.9

<sup>a</sup> IS: Isomer shift.<sup>b</sup> QS: quadrupole splitting.**Table 4**

Pd and Fe species on the different catalysts and their performances in the HDO of furan compounds under the investigated conditions.

Catalyst	Pd species	Fe species	Activity in HDO process
5%Pd/SiO <sub>2</sub>	Metallic Pd	–	Active
5%Pd-2.5%FeO <sub>x</sub> /SiO <sub>2</sub>	Metallic Pd, Pd-Fe alloy	Pd-Fe alloy, Fe <sup>II</sup> , Fe <sup>III</sup>	More active
10%FeO <sub>x</sub> /SiO <sub>2</sub>	–	Metallic Fe, Fe <sup>II</sup> , Fe <sup>III</sup>	Inactive

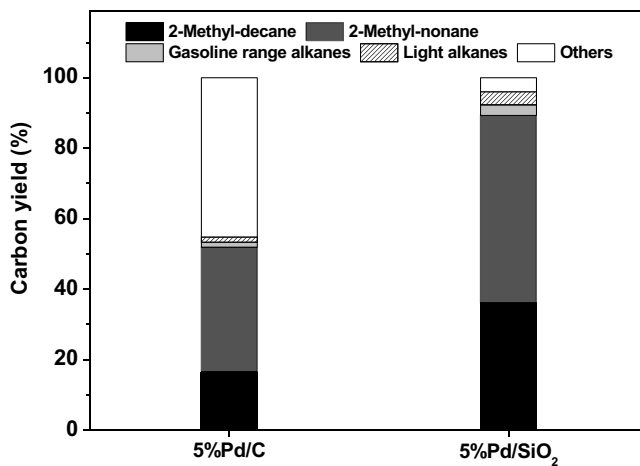


**Fig. 10.** Carbon yields of 2-methyl-decane, 2-methyl-nonane, C<sub>5</sub>–C<sub>7</sub> gasoline range alkanes, C<sub>1</sub>–C<sub>4</sub> light alkanes and other products from the hydrodeoxygenation (HDO) of **1A** over the 5%Pd/C and 5%Pd/SiO<sub>2</sub> catalysts. Reaction conditions: 623 K, 6 MPa H<sub>2</sub>; 1.8 g catalyst; liquid feedstock flow rate 0.04 mL min<sup>-1</sup>; hydrogen flow rate: 110 mL min<sup>-1</sup> at STP.

ketone (MIBK) [65] which can be obtained in industrial scale from lignocellulose. In this work, we chose this compound as a representative for furan-based diesel and jet fuel precursors and compared the HDO activities of a series of Pd catalysts. From Fig. 10, we can see that the support has strong influence on the solvent-free HDO of **1A** over Pd catalyst. Compared with the 5%Pd/C catalyst which has been used in our previous work [30], much higher carbon yield of alkanes (96.0% vs. 54.8%) were achieved over the 5%Pd/SiO<sub>2</sub> catalyst at 623 K and 6 MPa hydrogen pressure, which can be attributed to the higher Pd dispersion on the 5%Pd/SiO<sub>2</sub> catalyst than that on the 5%Pd/C catalyst (see Table S2 in supporting information). From this result, we can see that SiO<sub>2</sub> is better than active carbon to act as the support of Pd catalysts used in the HDO of **1A**. According to the analysis of GC-MS, the jet fuel range alkanes obtained in this work are mainly composed of 2-methyl-decane and 2-methyl-nonane. These branched alkanes have low freezing points (223.5 K and 198.3 K). Therefore, they can be blended into jet fuel without hydroisomerization. It is very interesting that the carbon yield (or selectivity) of 2-methyl-decane over the Pd/SiO<sub>2</sub> catalyst can be further improved after the modification of small amount of iron (see Fig. 11). Such a promotion effect is the most evident when the iron content in the Pd-FeO<sub>x</sub>/SiO<sub>2</sub> catalyst is about 2.5 wt.%. Beyond this value, the further increase of iron content to 5 wt.% will lead to the higher 2-methyl-decane/2-methyl-nonane ratio and the lower HDO activity

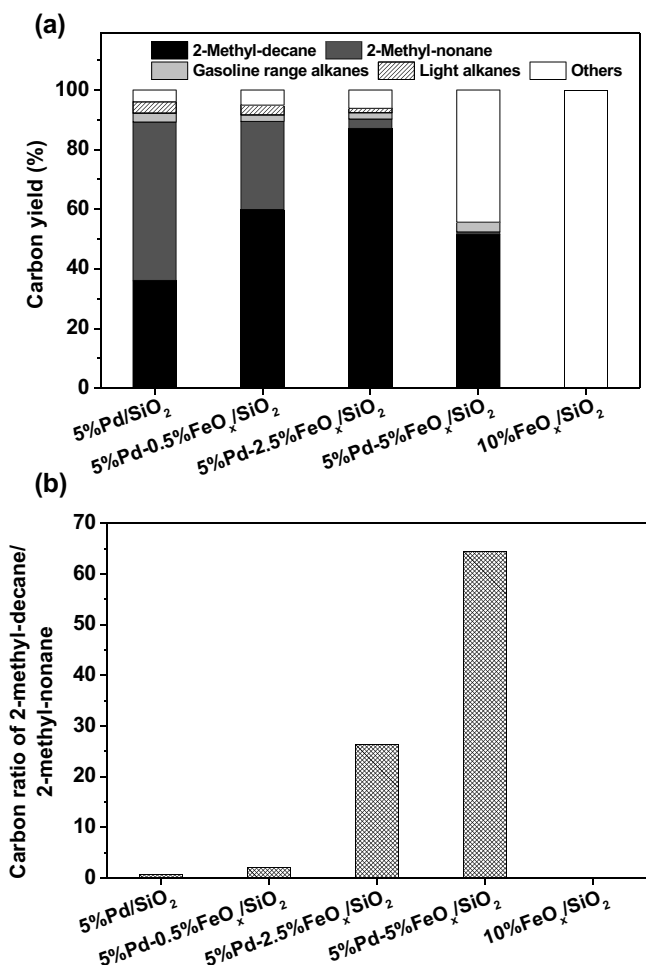


**Fig. 11.** Carbon yields of 2-methyl-decane, 2-methyl-nonane, C<sub>5</sub>–C<sub>7</sub> gasoline range alkanes, C<sub>1</sub>–C<sub>4</sub> light alkanes and other products (a) and carbon ratio of 2-methyl-decane/2-methyl-nonane (b) from the HDO of **1A** over the Pd/SiO<sub>2</sub>, Pd-FeO<sub>x</sub>/SiO<sub>2</sub> and FeO<sub>x</sub>/SiO<sub>2</sub> catalysts. Reaction conditions: 623 K, 6 MPa H<sub>2</sub>; 1.8 g catalyst, liquid feedstock flow rate 0.04 mL min<sup>-1</sup>, hydrogen flow rate: 110 mL min<sup>-1</sup> at STP.

of the catalyst. According to the STEM results (see Fig. 2), the lower HDO activity of 5%Pd-2.5%FeO<sub>x</sub>/SiO<sub>2</sub> catalyst can be explained by the aggregation of Pd-Fe alloy particles when iron content in the Pd-FeO<sub>x</sub>/SiO<sub>2</sub> catalyst is higher than 2.5 wt.%. Another promotion effect of iron species is to restrain the production of light alkanes

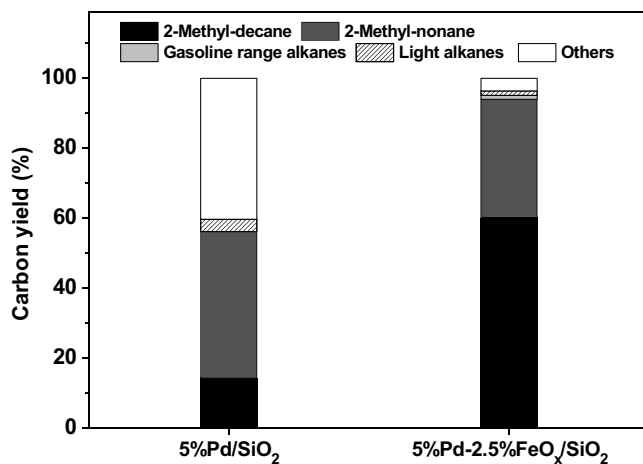


**Fig. 12.** Carbon yields of 2-methyl-decane, 2-methyl-nonane, C<sub>5</sub>–C<sub>7</sub> gasoline range alkanes, C<sub>1</sub>–C<sub>4</sub> light alkanes and other products from the HDO of **1A** over the 5%Pd/SiO<sub>2</sub> and 5%Pd-2.5%FeO<sub>x</sub>/SiO<sub>2</sub> catalysts under atmospheric pressure. Reaction conditions: 623 K, 0.1 MPa H<sub>2</sub>; 1.8 g catalyst, liquid feedstock flow rate 0.04 mL min<sup>-1</sup>, hydrogen flow rate: 110 mL min<sup>-1</sup> at STP.

which will also decrease the carbon yield of jet fuel range alkanes. In contrast, the 10%FeO<sub>x</sub>/SiO<sub>2</sub> catalyst is inactive for the solvent-free HDO of **1A** under the investigated condition.

Subsequently, we compared the activity of the 5%Pd/SiO<sub>2</sub> and 5%Pd-2.5%FeO<sub>x</sub>/SiO<sub>2</sub> catalysts for the solvent-free HDO of **1A** under atmospheric pressure. As we can see from Fig. 12, **1A** was totally converted over the 5%Pd-2.5%FeO<sub>x</sub>/SiO<sub>2</sub> catalyst at 623 K. High carbon yield of 2-methyl-decane and 2-methyl-nonane (94.0%) was achieved. In contrast, evidently lower carbon yield of 2-methyl-decane and 2-methyl-nonane (55.2%) was achieved over the 5%Pd/SiO<sub>2</sub> catalyst under the same conditions. According to the analysis of GC-MS (see Fig. S6 in supporting information), a series of oxygenates (such as 2-methylnonan-4-one, 2-methyldecan-4-one and 9-methyldecan-4-one) from the partial HDO of **1A** were identified in the liquid products over the 5%Pd/SiO<sub>2</sub> catalyst. These compounds can be considered as the intermediates between **1A** and 2-methyl-decane or 2-methyl-nonane.

To check the applicability of the Pd-FeO<sub>x</sub>/SiO<sub>2</sub> for the solvent-free HDO of other lignocellulosic furan compounds under atmospheric pressure, we also studied the solvent-free HDO of the **2A** (from the aldol condensation of 2-pentanone and furfural) and the **3A** (from the hydroxylalkylation/alkylation of 2-methylfuran and butanal) over the 5%Pd/SiO<sub>2</sub> and 5%Pd-2.5%FeO<sub>x</sub>/SiO<sub>2</sub> catalysts. As we can see from Fig. 13, significantly higher carbon yields of alkanes can be achieved over the 5%Pd-2.5%FeO<sub>x</sub>/SiO<sub>2</sub> catalyst than those obtained over the 5%Pd/SiO<sub>2</sub> catalyst. Considering the excellent performance of the Pd-FeO<sub>x</sub>/SiO<sub>2</sub>, we believe that it is a promising HDO catalyst in the future application.

#### 4. Discussion

According to the intermediates which were produced by the partial HDO of **1A** over the 5%Pd/SiO<sub>2</sub> catalyst under atmospheric pressure and some recent literature about the HDO mechanism of similar reaction system [31,66–70], the promotion effects of iron species on the selectivity of 2-methyl-decane over the Pd/SiO<sub>2</sub> catalyst may be rationalized by restraining the two C–C cleavage reactions which may occur during the HDO process: 1) The decarbonylation of aldehyde intermediates (*i.e.* the **1D** and **1F** in Scheme 2) generated by the hydrolysis of furan group (which will lead to the lower 2-methyl-decane/2-methyl-nonane ratio in the HDO products). 2) The retro-aldol condensation reaction which

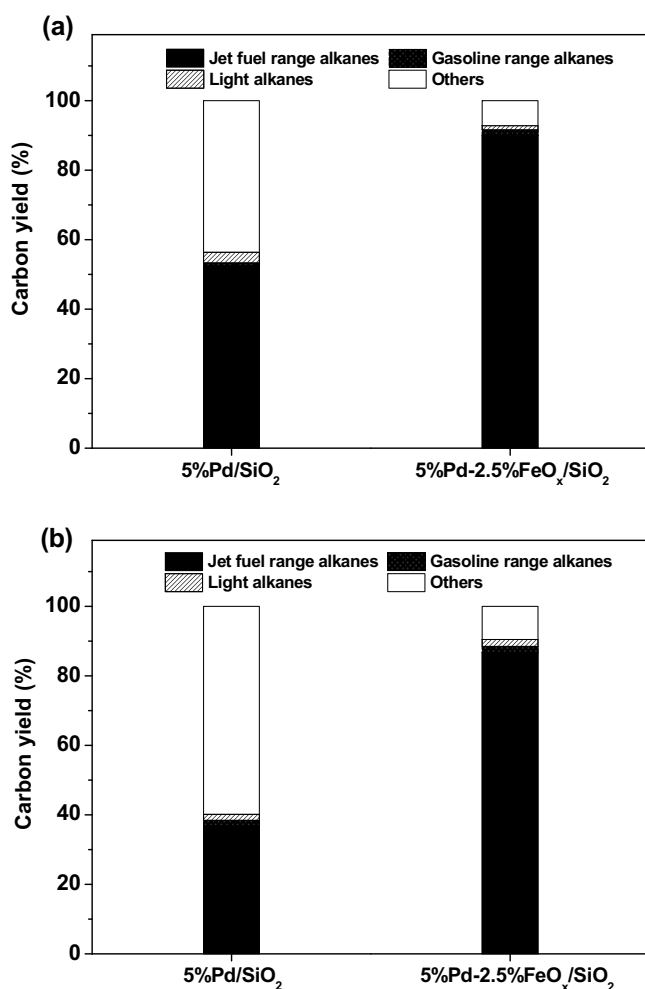


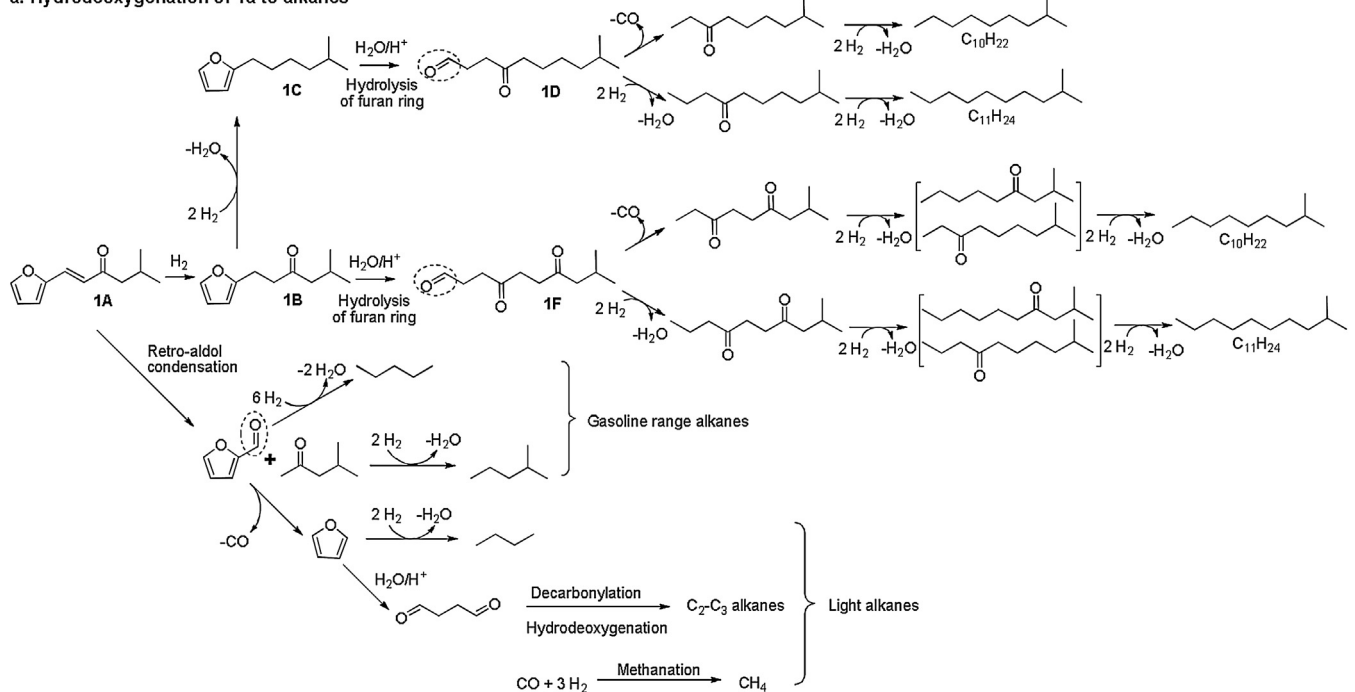
**Fig. 13.** Carbon yields of C<sub>9</sub>–C<sub>14</sub> jet fuel range alkanes, C<sub>5</sub>–C<sub>7</sub> gasoline range alkanes, C<sub>1</sub>–C<sub>4</sub> light alkanes and other products from the HDO of **2A** (a) and **3A** (b) over the 5%Pd/SiO<sub>2</sub> and 5%Pd-2.5%FeO<sub>x</sub>/SiO<sub>2</sub> catalysts under atmospheric pressure. Reaction conditions: 623 K (a), 573 K (b), 0.1 MPa H<sub>2</sub>; 1.8 g catalyst, liquid feedstock flow rate 0.04 mL min<sup>-1</sup>, hydrogen flow rate: 110 mL min<sup>-1</sup> at STP.

may lead to the generation of light alkanes (the reaction pathways for the generation of light alkanes were shown in Scheme 2).

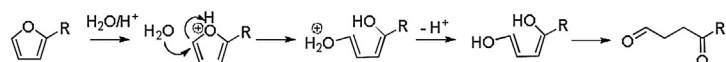
To prove the restraining effect of iron species on the decarbonylation and retro-aldol condensation, we compared the catalytic performances of the 5%Pd/SiO<sub>2</sub> and 5%Pd-2.5%FeO<sub>x</sub>/SiO<sub>2</sub> in the solvent-free HDO of 2-ethyl-2-hexenal (a lignocellulosic platform compound which can be obtained from the self-aldol condensation of butanal [71]). The reaction was carried out under the same reaction conditions as we used for the solvent-free HDO of **1A**. As we expected, n-heptane was obtained as the main product from the HDO of 2-ethyl-2-hexenal over the 5%Pd/SiO<sub>2</sub> catalyst, while 3-methyl-heptane was identified as the main product from the HDO of 2-ethyl-2-hexenal over the 5%Pd-2.5%FeO<sub>x</sub>/SiO<sub>2</sub> catalyst (see Fig. 14). Furthermore, it was also noticed that the carbon yield of light alkanes from the retro-aldol condensation during the HDO of 2-ethyl-2-hexenal over the 5%Pd-2.5%FeO<sub>x</sub>/SiO<sub>2</sub> catalyst (the reaction pathway was shown in Scheme 3) is also lower than that over the Pd/SiO<sub>2</sub> catalyst.

The restraining effect of iron species on the decarbonylation over Pd/SiO<sub>2</sub> catalyst can be explained by the adsorption mode of carbonyl group on the surface of catalyst. According to literature [72,73], two kinds of surface species can be formed after the adsorption of aldehyde on metal sites (see Fig. 15). One is the  $\eta^1$ -(O) surface species. The carbonyl group is bonded to one metal site

**a. Hydrodeoxygenation of 1a to alkanes**



**b. Hydrolysis of furan ring**



**Scheme 2.** Reaction pathways for the production of different alkanes from the hydrodeoxygenation (HDO) of **1A**.

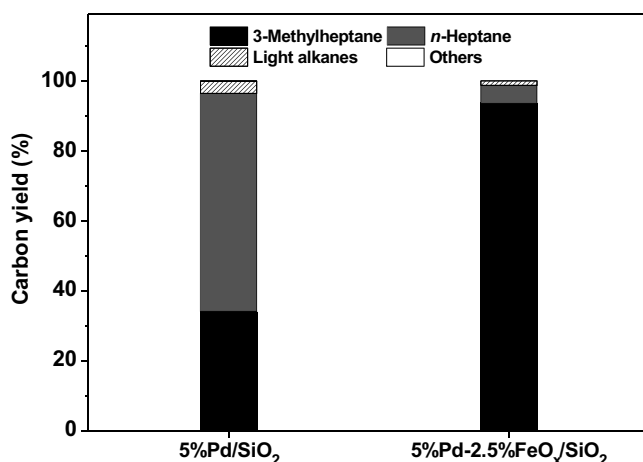
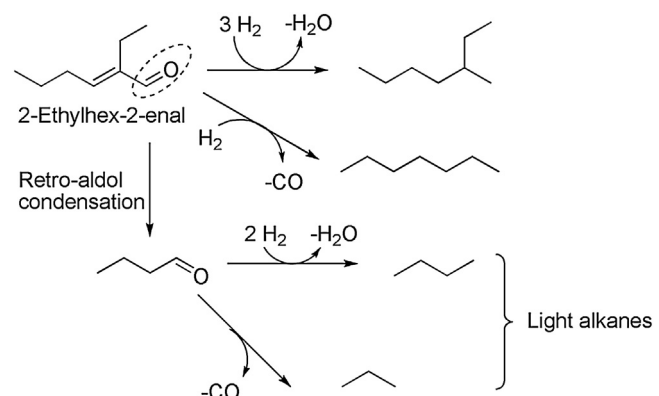


**Fig. 14.** Carbon yields of 3-methylheptane, *n*-heptane, C<sub>1</sub>–C<sub>4</sub> light alkanes and other products from the HDO of 2-ethylhex-2-enal over the 5%Pd/SiO<sub>2</sub> and 5%Pd–2.5%FeO<sub>x</sub>/SiO<sub>2</sub> catalysts. Reaction conditions: 623 K, 6 MPa H<sub>2</sub>; 1.8 g catalyst, liquid feedstock flow rate 0.04 mL min<sup>-1</sup>, hydrogen flow rate: 110 mL min<sup>-1</sup> at STP.

through the lone pair of oxygen atom. Another one is the  $\eta^2$ -(C, O) surface species. The C and O atoms of the carbonyl group interact with two adjacent metal sites. In the presence of hydrogen, the  $\eta^1$ -(O) surface species will be hydrogenated to alcohol and subsequently hydrodeoxygenated to alkanes at high temperature (route 1), while the  $\eta^2$ -(C, O) surface species may be transformed into a more stable acyl surface species which may decompose into alkanes and CO by decarbonylation reaction (route 2). In the recent work of Resasco group [72,73], it was found that the aldehydes adsorbed on Pd surface tend to form  $\eta^2$ -(C, O) surface intermediates. That may be the reason for the significant decarbonylation



**Scheme 3.** Reaction pathways for the production of different alkanes from the HDO of 2-ethylhex-2-enal

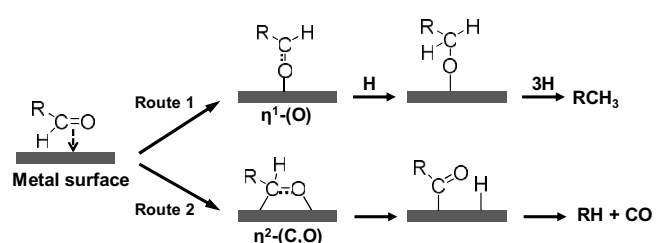


**Fig. 15.** Two reaction pathways for the deoxygenation of aldehyde over metal catalyst.

during the HDO of aldehydes (such as 2-ethyl-2-hexenal) over the Pd/SiO<sub>2</sub> catalyst. From what we observed by the FT-IR spectra with CO as the probe molecule, the modification of iron species decreases

the coordination number of Pd–Pd on the Pd/SiO<sub>2</sub> catalyst and makes Pd sites on the Pd–FeO<sub>x</sub>/SiO<sub>2</sub> catalyst more isolated. As the result, the linearly adsorbed CO predominates over bridge bonded CO on the Pd–FeO<sub>x</sub>/SiO<sub>2</sub> catalyst. Analogously, for the adsorption of carbonyl compounds, the formation of  $\eta^2$ -(C, O) surface intermediate which needs two adjacent Pd atoms is restrained in the presence of iron species (due to the lower coordination number of Pd–Pd on the Pd–FeO<sub>x</sub>/SiO<sub>2</sub> catalyst). This may be the reason for less C–C cleavage by decarbonylation over the Pd–FeO<sub>x</sub>/SiO<sub>2</sub> catalyst. The influence of iron species on the coordination number of Pd–Pd on the Pd/SiO<sub>2</sub> catalyst can be explained by two reasons: 1) Dilution effect caused by the formation of Pd–Fe alloy. 2) The coverage of Pd (or Pd–Fe alloy) particles with FeO<sub>x</sub> clusters which will lead to the generation of lower coordinated Pd sites at the interfaces of metal particles and FeO<sub>x</sub> clusters. The restraining effect of iron species on the retro-aldol condensation over Pd/SiO<sub>2</sub> catalyst can be explained by the higher activity of Pd–Fe alloy than Pd for the hydrogenation of carbonyl group. As we know, aldol condensation is a reversible reaction. According to the literature about reaction mechanism for the HDO of biomass derived oxygenates [52], the retro-aldol condensation can be restrained by the hydrogenation of carbonyl group. In the recent work of Huber et al. [74], it was found that the modification of Pd catalyst with iron species can significantly increase its activity for the hydrogenation of carbonyl compounds (such as xylose). This may be the reason why the carbon yields of light alkanes from the HDO of **1A**, **2A** and 2-ethyl-2-hexenal over the 5%Pd–2.5%FeO<sub>x</sub>/SiO<sub>2</sub> catalyst are evidently lower than those over the 5%Pd/SiO<sub>2</sub> catalyst (see Figs. 11–14).

**Table 4** compared the Pd and Fe species which were identified on the 5%Pd/SiO<sub>2</sub>, 5%Pd–2.5%FeO<sub>x</sub>/SiO<sub>2</sub> and 10%FeO<sub>x</sub>/SiO<sub>2</sub> catalysts by XRD, STEM, H<sub>2</sub>-TPR, EXAFS, *in-situ* XPS and *quasi-in-situ* Mössbauer analysis. From it, we can see that the 5%Pd/SiO<sub>2</sub> catalyst which contains metallic Pd as the only Pd species is active for the HDO of furan compounds. The modification of Pd/SiO<sub>2</sub> catalyst with iron species leads to the generation of Pd–Fe alloy, partially reduced FeO<sub>x</sub> species and the much higher HDO activity of catalyst under atmospheric pressure. According to the CO chemisorption result, the presence of iron species leads to the decrease of chemically accessible Pd sites on the surface of Pd/SiO<sub>2</sub> catalyst. Therefore, we can't attribute the promoting effect of iron species to higher amount of metal sites. The 10%FeO<sub>x</sub>/SiO<sub>2</sub> catalyst (with metallic Fe, Fe<sup>II</sup>, and Fe<sup>III</sup> as the surface species) is totally inactive for the HDO of furan compounds under the investigated conditions. Based on these results, we believe the generation of Pd–Fe alloy or the synergism effect between Pd–Fe alloy and the partially reduced FeO<sub>x</sub> species may be the reason for the excellent performance of Pd–FeO<sub>x</sub>/SiO<sub>2</sub> catalyst for the solvent-free HDO of furan compounds under atmospheric pressure.

**Pd–Fe alloy effect:** Due to the D-band effect, alloy sites are more active than mono metal sites for many hydrogenation or hydrogenolysis reactions [75]. In the recent work of Resasco et al. [76], it was found that Ni–Fe alloy is more active than Ni for the hydrogenolysis of carbonyl group and furan ring. They attributed the higher HDO activity of Ni–Fe alloy to the strong interaction of oxygenates with the oxyphilic Fe atoms. In the previous work of Pinna [54], bimetallic Pd–Fe/SiO<sub>2</sub> catalyst was found to be more active than Pd/SiO<sub>2</sub> catalyst for the hydrogenation of 2,4-dinitrotoluene. Analogously, we think that the formation of Pd–Fe alloy may be one reason for the higher HDO activity of Pd–FeO<sub>x</sub>/SiO<sub>2</sub> catalysts.

**Synergism effect of the metal particle and FeO<sub>x</sub> species:** In some recent literature about the hydrogenolysis of biomass derived oxygenates (such as tetrahydrofurfuryl alcohol [77–79], carboxylic acid [55,80–82] and polyols [83–85]), evident synergism effects were observed between the noble metal particles and the partially reduced transition metal oxide which are attached on them. It was

suggested the presence of partially reduced metal oxide will promote the adsorption of oxygen-containing functional group and the following C–O bond cleavage by hydrogenolysis. There is another possibility: Similar to what has been found by Wang et al. in their previous work about the HDO over Pd/Nb<sub>2</sub>O<sub>5</sub>/SiO<sub>2</sub> catalyst [39], the partial reduction of FeO<sub>x</sub> species will also lead to the generation of oxygen vacancy which may be favorable for the C–O cleavage by the Mars–van Krevelen mechanism [61,86]. Analogously, the close contact of Pd–Fe alloy (or Pd) particles and FeO<sub>x</sub> species in the Pd–FeO<sub>x</sub>/SiO<sub>2</sub> catalyst is beneficial for the generation of partially reduced iron species by hydrogen spillover, which may facilitate the C–O cleavage and improve the HDO activity of catalyst.

## 5. Conclusions

Pd–FeO<sub>x</sub>/SiO<sub>2</sub> was found to be an active catalyst for the solvent-free hydrodeoxygenation (HDO) of furan compounds under atmospheric pressure. Over the 5%Pd–2.5%FeO<sub>x</sub>/SiO<sub>2</sub> catalyst, complete conversion of feedstocks and high carbon yields of jet fuel range alkanes (87–94%) can be achieved by the atmospheric HDO of a series of furan compounds at 623 K or 573 K. The modification of iron species decreases the coordination number of Pd–Pd on the Pd/SiO<sub>2</sub> catalyst and hinders the formation  $\eta^2$ -(C, O) surface species (which needs at least two adjacent Pd atoms). As a result, the decarbonylation reaction (which will lead to the lower carbon yield of jet fuel range alkanes) during the HDO process is restrained. Another function of iron species is to promote the hydrogenation of carbonyl group over Pd, which can restrain the retro-aldol condensation and the formation of shorter chain alkanes. The modification of Pd/SiO<sub>2</sub> with iron species also leads to the generation of Pd–Fe alloy and partially reduced FeO<sub>x</sub> species. Both effects may be the reasons why the HDO activity of the Pd–FeO<sub>x</sub>/SiO<sub>2</sub> catalyst is higher than that of the Pd/SiO<sub>2</sub> catalyst under atmospheric pressure.

## Acknowledgments

This work is supported by the Natural Science Foundation of China (No. 21277140; 21476229; 21506213), Dalian Science Foundation for Distinguished Young Scholars (No. 2015R005), the Strategic Priority Research Program of the Chinese Academy of Sciences (XDB17020100) and 100-talent project of Dalian Institute of Chemical Physics (DICP). The authors thank the staffs in beamline 14W1 of the Shanghai synchrotron radiation facility (SSRF) for their great help on measurements and data analyses of EXAFS.

## Appendix A. Supplementary data

Supplementary data associated with this article can be found, in the online version, at <http://dx.doi.org/10.1016/j.apcatb.2016.08.045>.

## References

- [1] G.W. Huber, S. Iborra, A. Corma, Chem. Rev. 106 (2006) 4044–4098.
- [2] D.M. Alonso, J.Q. Bond, J.A. Dumesic, Green Chem. 12 (2010) 1493–1513.
- [3] M.J. Climent, A. Corma, S. Iborra, Green Chem. 16 (2014) 516–547.
- [4] Q. Xia, Z. Chen, Y. Shao, X. Gong, H. Wang, X. Liu, S.F. Parker, X. Han, S. Yang, Y. Wang, Nat. Commun. 7 (2016) 11162.
- [5] K. Bartha, P.C. Ford, Acc. Chem. Res. 47 (2014) 1503–1512.
- [6] A. Corma, S. Iborra, A. Velty, Chem. Rev. 107 (2007) 2411–2502.
- [7] M. Besson, P. Gallezot, C. Pinel, Chem. Rev. 114 (2014) 1827–1870.
- [8] F. Liu, M. Audemar, K. De Oliveira Vigier, J.-M. Clacens, F. De Campo, F. Jerome, Green Chem. 16 (2014) 4110–4114.
- [9] W.P. Deng, Y.L. Wang, Q.H. Zhang, Y. Wang, Catal. Surv. Asia 16 (2012) 91–105.
- [10] Y. Nakagawa, K. Tomishige, Catal. Surv. Asia 15 (2011) 111–116.
- [11] S. Crossley, J. Faria, M. Shen, D.E. Resasco, Science 327 (2010) 68–72.
- [12] G.W. Huber, J.N. Chheda, C.J. Barrett, J.A. Dumesic, Science 308 (2005) 1446–1450.

[13] P. Anbarasan, Z.C. Baer, S. Sreekumar, E. Gross, J.B. Binder, H.W. Blanch, D.S. Clark, F.D. Toste, *Nature* 491 (2012) 235–239.

[14] B.G. Harvey, R.L. Quintana, *Energy Environ. Sci.* 3 (2010) 352–357.

[15] S. Sankaranarayananpillai, S. Sreekumar, J. Gomes, A. Grippo, G.E. Arab, M. Head-Gordon, F.D. Toste, A.T. Bell, *Angew. Chem. Int. Ed.* 54 (2015) 4673–4677.

[16] E.R. Sacia, M.H. Deaner, Y. Louie, A.T. Bell, *Green Chem.* 17 (2015) 2393–2397.

[17] E.L. Kunkes, D.A. Simonetti, R.M. West, J.C. Serrano-Ruiz, C.A. Gartner, J.A. Dumesic, *Science* 322 (2008) 417–421.

[18] J.Q. Bond, D.M. Alonso, D. Wang, R.M. West, J.A. Dumesic, *Science* 327 (2010) 1110–1114.

[19] J.Q. Bond, A.A. Upadhye, H. Olcay, G.A. Tompsett, J. Jae, R. Xing, D.M. Alonso, D. Wang, T. Zhang, R. Kumar, A. Foster, S.M. Sen, C.T. Maravelias, R. Malina, S.R.H. Barrett, R. Lobo, C.E. Wyman, J.A. Dumesic, G.W. Huber, *Energy Environ. Sci.* 7 (2014) 1500–1523.

[20] R. Xing, A.V. Subrahmanyam, H. Olcay, W. Qi, G.P. van Walsum, H. Pendse, G.W. Huber, *Green Chem.* 12 (2010) 1933–1946.

[21] H. Olcay, A.V. Subrahmanyam, R. Xing, J. Lajoie, J.A. Dumesic, G.W. Huber, *Energy Environ. Sci.* 6 (2013) 205–216.

[22] A.V. Subrahmanyam, S. Thayumanavan, G.W. Huber, *ChemSusChem* 3 (2010) 1158–1161.

[23] A. Corma, O. de la Torre, M. Renz, N. Villandier, *Angew. Chem. Int. Ed.* 50 (2011) 2375–2378.

[24] A. Corma, O. de la Torre, M. Renz, *ChemSusChem* 4 (2011) 1574–1577.

[25] A. Corma, O. de la Torre, M. Renz, *Energy Environ. Sci.* 5 (2012) 6328–6344.

[26] K.S. Arias, M.J. Climent, A. Corma, S. Iborra, *Energy Environ. Sci.* 8 (2015) 317–331.

[27] G. Li, N. Li, Z. Wang, C. Li, A. Wang, X. Wang, Y. Cong, T. Zhang, *ChemSusChem* 5 (2012) 1958–1966.

[28] D. Liu, E.Y.X. Chen, *ChemSusChem* 6 (2013) 2236–2239.

[29] G. Li, N. Li, S. Li, A. Wang, Y. Cong, X. Wang, T. Zhang, *Chem. Commun.* 49 (2013) 5727–5729.

[30] J. Yang, N. Li, G. Li, W. Wang, A. Wang, X. Wang, Y. Cong, T. Zhang, *ChemSusChem* 6 (2013) 1149–1152.

[31] Q.-N. Xia, Q. Cuan, X.-H. Liu, X.-Q. Gong, G.-Z. Lu, Y.-Q. Wang, *Angew. Chem. Int. Ed.* 53 (2014) 9755–9760.

[32] C. Wen, E. Barrow, J. Hattrick-Simpers, J. Lauterbach, *Phys. Chem. Chem. Phys.* 16 (2014) 3047–3054.

[33] J. Yang, N. Li, S. Li, W. Wang, L. Li, A. Wang, X. Wang, Y. Cong, T. Zhang, *Green Chem.* 16 (2014) 4879–4884.

[34] S. Sreekumar, M. Balakrishnan, K. Goulas, G. Gunbas, A.A. Gokhale, L. Louie, A. Grippo, C.D. Scown, A.T. Bell, F.D. Toste, *ChemSusChem* 8 (2015) 2609–2614.

[35] Q. Deng, P.J. Han, J.S. Xu, J.J. Zou, L. Wang, X.W. Zhang, *Chem. Eng. Sci.* 138 (2015) 239–243.

[36] A.D. Sutton, F.D. Waldie, R.L. Wu, M. Schlaf, L.A. Silks, J.C. Gordon, *Nat. Chem.* 5 (2013) 428–432.

[37] W. Xu, Q. Xia, Y. Zhang, Y. Guo, Y. Wang, G. Lu, *ChemSusChem* 4 (2011) 1758–1761.

[38] C.R. Waidmann, A.W. Pierpont, E.R. Batista, J.C. Gordon, R.L. Martin, L.A. Silks, R.M. West, R.L. Wu, *Catal. Sci. Tech.* 3 (2013) 106–115.

[39] Y. Shao, Q. Xia, X. Liu, G. Lu, Y. Wang, *ChemSusChem* 8 (2015) 1761–1767.

[40] M. Grilc, B. Likozar, J. Levec, *ChemCatChem* 8 (2016) 180–191.

[41] M. Grilc, B. Likozar, J. Levec, *Appl. Catal. B: Environ.* 150–151 (2014) 275–287.

[42] M. Grilc, B. Likozar, J. Levec, *Biomass Bioenergy* 63 (2014) 300–312.

[43] G.W. Huber, A. Corma, *Angew. Chem. Int. Ed.* 46 (2007) 7184–7201.

[44] G.W. Huber, P. O'Connor, A. Corma, *Appl. Catal. A: Gen.* 329 (2007) 120–129.

[45] G. Veryasov, M. Grilc, B. Likozar, A. Jesih, *Catal. Commun.* 46 (2014) 183–186.

[46] T.B. Celic, M. Grilc, B. Likozar, N.N. Tusar, *ChemSusChem* 8 (2015) 1703–1710.

[47] M. Grilc, G. Veryasov, B. Likozar, A. Jesih, J. Levec, *Appl. Catal. B: Environ.* 163 (2015) 467–477.

[48] B. Ravel, M. Newville, *J. Synchrotron Radiat.* 12 (2005) 537–541.

[49] G. Li, N. Li, J. Yang, L. Li, A. Wang, X. Wang, Y. Cong, T. Zhang, *Green Chem.* 16 (2014) 594–599.

[50] S. Li, N. Li, G. Li, L. Li, A. Wang, Y. Cong, X. Wang, T. Zhang, *Green Chem.* 17 (2015) 3644–3652.

[51] S. Li, N. Li, G. Li, L. Li, A. Wang, Y. Cong, X. Wang, G. Xu, T. Zhang, *Appl. Catal. B: Environ.* 170–171 (2015) 124–134.

[52] N. Li, G.W. Huber, *J. Catal.* 270 (2010) 48–59.

[53] B. Qiao, A. Wang, X. Yang, L.F. Allard, Z. Jiang, Y. Cui, J. Liu, J. Li, T. Zhang, *Nat. Chem.* 3 (2011) 634–641.

[54] F. Pinna, M. Selva, M. Signoretto, G. Strukul, F. Bocchetti, A. Benedetti, P. Canton, G. Fagherazzi, *J. Catal.* 150 (1994) 356–367.

[55] Z. Wang, G. Li, X. Liu, Y. Huang, A. Wang, W. Chu, X. Wang, N. Li, *Catal. Commun.* 43 (2014) 38–41.

[56] B. Pholjaroen, N. Li, Y. Huang, L. Li, A. Wang, T. Zhang, *Catal. Today* 245 (2015) 93–99.

[57] F. Bocchetti, E. Guglielminotti, F. Pinna, M. Signoretto, *J. Chem. Soc. Faraday Trans.* 91 (1995) 3237–3244.

[58] J. Lin, B. Qiao, J. Liu, Y. Huang, A. Wang, L. Li, W. Zhang, L.F. Allard, X. Wang, T. Zhang, *Angew. Chem. Int. Ed.* 51 (2012) 2920–2924.

[59] G. Lielitz, M. Nizm, J. Völter, K. Lázár, L. Guczi, *Appl. Catal.* 45 (1988) 71–83.

[60] E.E. Unmuth, L.H. Schwartz, J.B. Butt, *J. Catal.* 61 (1980) 242–255.

[61] A.J.R. Hensley, Y. Hong, R. Zhang, H. Zhang, J. Sun, Y. Wang, J.-S. McEwen, *ACS Catal.* 4 (2014) 3381–3392.

[62] Y. Hong, H. Zhang, J. Sun, K.M. Ayman, A.J.R. Hensley, M. Gu, M.H. Engelhard, J.-S. McEwen, Y. Wang, *ACS Catal.* 4 (2014) 3335–3345.

[63] R.L. Garten, *J. Catal.* 43 (1976) 18–33.

[64] J.-P. Lange, E. van der Heide, J. van Buijtenen, R. Price, *ChemSusChem* 5 (2012) 150–166.

[65] P. Wang, S. Bai, J. Zhao, P. Su, Q. Yang, C. Li, *ChemSusChem* 5 (2012) 2390–2396.

[66] L. Faba, E. Díaz, S. Ordóñez, *Appl. Catal. B: Environ.* 160–161 (2014) 436–444.

[67] B.L. Wegenhart, L. Yang, S.C. Kwan, R. Harris, H.I. Kenttämaa, M.M. Abu-Omar, *ChemSusChem* 7 (2014) 2742–2747.

[68] L. Faba, E. Diaz, S. Ordóñez, *Catal. Sci. Tech.* 5 (2015) 1473–1484.

[69] Y. Li, X. Huang, Q. Zhang, L. Chen, X. Zhang, T. Wang, L. Ma, *Appl. Energy* 160 (2015) 990–998.

[70] R. Ramos, Z. Tisler, O. Kikhtyanin, D. Kubicka, *Catal. Sci. Tech.* 6 (2016) 1829–1841.

[71] W.Q. Shen, G.A. Tompsett, R. Xing, W.C. Conner, G.W. Huber, *J. Catal.* 286 (2012) 248–259.

[72] S. Sitthisa, D.E. Resasco, *Catal. Lett.* 141 (2011) 784–791.

[73] S. Sitthisa, T. Pham, T. Prasomsri, T. Sooknoi, R.G. Mallinson, D.E. Resasco, *J. Catal.* 280 (2011) 17–27.

[74] J. Lee, Y.T. Kim, G.W. Huber, *Green Chem.* 16 (2014) 708–718.

[75] W. Yu, M.D. Porosoff, J.G. Chen, *Chem. Rev.* 112 (2012) 5780–5817.

[76] S. Sitthisa, W. An, D.E. Resasco, *J. Catal.* 284 (2011) 90–101.

[77] S. Koso, I. Furikado, A. Shimaoto, T. Miyazawa, K. Kunimori, K. Tomishige, *Chem. Commun.* 45 (2009) 2035–2037.

[78] K. Chen, K. Mori, H. Watanabe, Y. Nakagawa, K. Tomishige, *J. Catal.* 294 (2012) 171–183.

[79] S. Koso, Y. Nakagawa, K. Tomishige, *J. Catal.* 280 (2011) 221–229.

[80] M. Li, G. Li, N. Li, A. Wang, W. Dong, X. Wang, Y. Cong, *Chem. Commun.* 50 (2014) 1414–1416.

[81] Y. Takeda, T. Shoji, H. Watanabe, M. Tamura, Y. Nakagawa, K. Okumura, K. Tomishige, *ChemSusChem* 8 (2015) 1170–1178.

[82] L. Corbel-Demalay, B.-K. Ly, D.-P. Minh, B. Tapin, C. Espel, F. Epron, A. Cabioc, E. Guillon, M. Besson, C. Pinel, *ChemSusChem* 6 (2013) 2388–2395.

[83] Y. Amada, S. Koso, Y. Nakagawa, K. Tomishige, *ChemSusChem* 3 (2010) 728–736.

[84] Y. Amada, H. Watanabe, Y. Hirai, Y. Kajikawa, Y. Nakagawa, K. Tomishige, *ChemSusChem* 5 (2012) 1991–1999.

[85] N. Ota, M. Tamura, Y. Nakagawa, K. Okumura, K. Tomishige, *Angew. Chem. Int. Ed.* 54 (2015) 1897–1900.

[86] T. Prasomsri, T. Nimmanwudipong, Y. Roman-Leshkov, *Energy Environ. Sci.* 6 (2013) 1732–1738.